Spectrum of single bunch longitudinal dipole modes

Nathan Towne and Jiunn-Ming Wang
National Synchrotron Light Source, Brookhaven National Laboratory, Upton, New York 11973
(Received 6 October 1997)

A mode of coherent longitudinal dipole motion of the beam in the National Synchrotron Light Source (NSLS) vacuum ultraviolet (vuv) ring with small frequency is observed by Biscardi *et al.* [Rev. Sci. Instrum. **66**, 1856 (1995)]. We point out in this paper that the coherent motion observed is, although a solution to the well-known secular equation for Robinson instability, a distinct mode of beam dipole motion from what is normally known as the Robinson mode. In this paper the mode's properties and its relationships with the usual Robinson mode are developed. The collision of the two modes is understood analytically and observed experimentally in the NSLS vuv ring. [S1063-651X(98)12503-5]

PACS number(s): 29.27.Bd

I. INTRODUCTION

Biscardi, Ramirez, Williams, and Zimba found [1] in 1995 that the quality of the infrared photon beam in the vacuum ultraviolet (vuv) ring of the National Synchrotron Light Source (NSLS) is degraded by a longitudinal coherent motion of the electron beam at about 5 kHz or less. They also found that the frequency of this coherent signal depends very much on the rf cavity detuning angle and thus they were able to minimize the photon beam degradation by making the rf cavity operation point more capacitive. The behavior of this coherent mode remained a puzzle since the frequency of the normal Robinson instability equals approximately the synchrotron frequency [2,3], and the synchrotron frequency of the vuv ring is about 10 kHz or more. Furthermore, the frequency of the Robinson mode in the vuv ring is known to increase with beam current [4]. Figure 1 shows both the Robinson dipole and quadrupole modes together with this unusual mode.

We point out in this paper that the coherent motion observed by Biscardi *et al.* is a distinct mode of beam dipole motion from what is normally known as the Robinson mode and yet this mode is also a solution to the well-known secular equation [5,6] for Robinson instability. We will refer in this paper to the conventional Robinson mode as the ''beam Robinson mode'' or the ''beam mode'' and to the second mode as the ''cavity Robinson mode'' or the ''cavity mode.'' We know from the work of Robinson that the (angular) frequency of the beam mode approaches the synchrotron frequency ω_s in the limit of vanishing average beam current. On the other hand, the frequency of the cavity mode approaches $\Delta + j\Gamma$ in the same limit, where $\Delta \equiv h\omega_0 - \omega_{res}$ is the frequency detuning, $\Gamma \equiv \omega_{res}/2Q$ is the cavity resonance mode damping rate, ω_0 is the revolution frequency, ω_{res} is the cavity resonance frequency, and h is the cavity harmonic number.

The beam coherent motion is associated with a feedback mechanism between the beam and the beam-induced electromagnetic fields in the storage ring; the coupling of the two is described by the beam impedance Z or equivalently by its Fourier transform W, the wake potential. If the rf cavity fundamental mode is the only source of the impedance, then the feedback is between two oscillators. For simplicity, we shall consider only this case in this paper.

This paper is organized in the following manner. In Sec. II we derive the characteristic equation for the frequency of the coherent longitudinal dipole motion of the beam, first more generally in the Z-transform space and then for the more special case where $|\Omega T_0| \ll 1$, where $T_0 = 2\pi/\omega_0$ is the revolution period and Ω is the coherent frequency.

In Sec. III we apply Routh criteria [7] to our model and find that the two nontrivial threshold conditions are the threshold condition of the resistive Robinson instability and the threshold condition for the reactive Robinson instability. Because Routh criteria are necessary and sufficient conditions, we have to consider only the resistive and the reactive

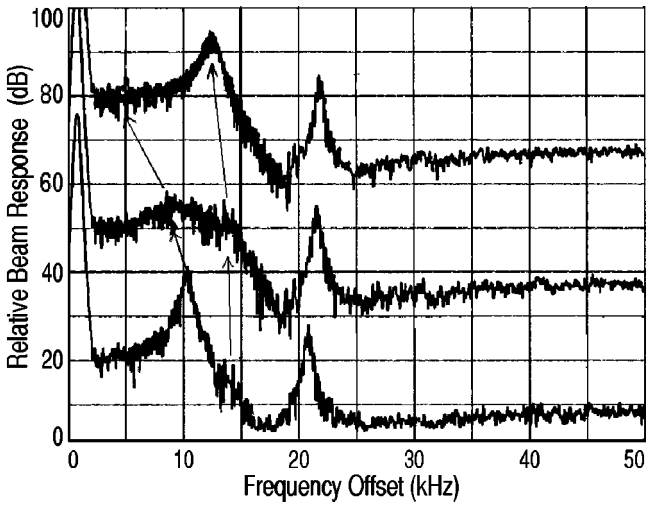

FIG. 1. Upper synchrotron sidebands of a rotation line for a 52-mA single bunch beam in the NSLS vuv ring. From top trace to bottom the cavity detunings are 2.5, 5.6, and 10.4 kHz below the generator frequency. The sidebands were observed on a spectrum analyzer and the coherent motion was excited using a broadband cavity driven by a tracking generator synchronized with the spectrum analyzer. The arrows show the progression of the two resonances arising from coherent dipole motion. The continuity of the resonances from trace to trace was verified using smaller increments of the cavity detuning. A quadrupole mode is also present at 21-kHz offset.

TABLE I. NSLS vuv ring parameters used in the numerical examples shown in the figures.

Parameter	Value
energy	0.744 GeV
momentum compaction (α)	0.0245
revolution frequency ($\omega_0/2\pi$)	5.876 MHz
peak operating current	
multiple bunch operation	0.85 A ($0.9\times10^{12}e^-$)
single bunch operation	0.4 A ($0.43\times10^{12}e^-$)
energy loss per turn (eV_γ)	14.4 keV
rf harmonic number (h)	9
rf peak voltage ($\hat{V}$)	78 kV
incoherent synchrotron	
frequency (ω_s)	$2\pi\times11.2$ kHz
cavity R/Q	125/2Ω
cavity Q	8460

Robinson coherent motion. (The Robinson condition is the condition that the coherent beam dipole motion loses phase focusing. The component of the coherent voltage that is reactive with respect to the beam current is responsible for such phase focusing.)

For certain values of the current and the detuning, $I=\overline{I}$ and $\Delta=\overline{\Delta}$, the coherent frequencies of the beam mode and the cavity mode may collide at $\Omega=\overline{\Omega}$. In Sec. IV the condition for such a collision is investigated and the expressions for $\overline{\Omega}$, $\overline{\Delta}$, and $\overline{I}$ are found. We present observational evidence from the vuv ring of the collision.

Section V deals with loci of solutions of the characteristic equation in the complex Ω plane, each locus corresponding to a given value of Δ and a range of the beam current I. The locus corresponding to $\Delta\rightarrow\overline{\Delta}$ is referred to as the confluence locus or the confluence curve. This curve passes through $\overline{\Omega}$ and it provides us with a convenient and visual means of classifying the beam and cavity modes. The Robinson condition for the beam and cavity modes in the vuv ring is discussed graphically.

All numerical examples in this paper are based on the parameters of the vuv ring; the parameters are given in Table I. Note that the total cavity voltage is kept fixed; as a result, the incoherent synchrotron frequency is fixed at 11.2 kHz. A detailed report describing the Robinson modes in the vuv ring is given elsewhere [8].

II. CHARACTERISTIC EQUATION FOR DIPOLE MOTION

First, we set up the equations for the coherent longitudinal dipole motion of a bunch. Consider a pointlike bunch with charge eN moving on the orbit $\theta=\omega_0 t+\phi(t)$, where θ is the azimuthal angle describing the position around the ring and ϕ is the bunch location relative to the synchronous position. We assume the rf cavity to be located at $\theta=0$, use the notation $t_p=pT_0+\tau_p$, where $T_0=2\pi/\omega_0$ is the revolution period, for the instant the bunch passes the cavity on its pth turn, and let ϕ_p be the value of ϕ at this instant. Clearly, $\phi_p=-\omega_0\tau_p$. Also define ϵ_p to be the value of $\epsilon\equiv(E-E_0)/E_0$ just before the bunch crosses the cavity on its pth turn. Then the equations of motion are

$$\phi_k-\phi_{k-1}=-2\pi\alpha\epsilon_k, \tag{1}$$

$$\epsilon_{k+1}-\epsilon_k=e[V(kT_0+\tau_k)-V_\gamma]/E_0, \tag{2}$$

where α is the momentum compaction factor, eV_γ is the radiation energy per particle per turn, and $V(t)=V_g(t)+V_b(t)$, with V_g being the generator voltage and V_b the beam-induced voltage. V_b is, in terms of the wake potential,

$$V_b(t)=-eN\sum_{p=-\infty}^{\infty}W(t-pT_0-\tau_p). \tag{3}$$

To the leading order in ϕ, the above equations lead to

$$\phi_{k+1}-2\phi_k+\phi_{k-1}=-T_0^2\omega_s^2\phi_k+\frac{e\omega_0\alpha}{2\pi E_0}eN\times\sum_{p=-\infty}^{k}\phi_p\dot{W}(kT_0-pT_0), \tag{4}$$

with

$$\omega_s^2=\frac{e\omega_0^2\alpha}{2\pi E_0}h\hat{V}\sin\psi_V, \tag{5}$$

where ψ_V is the phase of the cavity voltage relative to the beam, $\hat{V}$ is the magnitude of the voltage, $\dot{W}$ is the time derivative of W, and ω_s is the incoherent synchrotron frequency. Equation (4) is a homogeneous linear equation of ϕ_k. Setting $\phi_k=z^k$, we obtain

$$z-2+z^{-1}=-T_0^2\left[\omega_s^2-\frac{e\alpha}{E_0}I\sum_{p=0}^{\infty}z^{-p}\dot{W}(pT_0)\right], \tag{6}$$

where the average beam current $I=eN\omega_0/2\pi$. The summation is the Z transform of $\dot{W}$.

From now on, we consider the simplest case where the rf cavity fundamental mode is the only source of the impedance: For $t>0$,

$$W(t)=2k_0\cos\omega_{res}t\,\exp(-\Gamma t), \tag{7}$$

where the loss factor k_0 is the product of Γ with the shunt impedance R_{sh}. In this case, the Z transform of $\dot{W}$ is a rational function of z; Eq. (6) becomes

$$z-2+z^{-1}+T_0^2\omega_s^2=jk_0\frac{\alpha e}{E_0}T_0^2Iz\left[\frac{\omega_c}{z-z_c}-\frac{\omega_c^*}{z-z_c^*}\right], \tag{8}$$

where $z_c=e^{j\omega_c T_0}$ and the complex resonance frequency $\omega_c\equiv\omega_{res}+j\Gamma$. Additional rf modes add similar terms to the right-hand side of Eq. (8). Equation (8) is trivially converted to a polynomial equation in z,

$$z(z-2+z^{-1}+T_0^2\omega_s^2)(z-z_c)(z-z_c^*)=jk_0\frac{\alpha e}{E_0}T_0^2Iz^2[\omega_c(z-z_c^*)-\omega_c^*(z-z_c)], \tag{9}$$

an equation that is valid for arbitrary detuning of the cavity.

In the case that $|\Omega T_0| \ll 1$, to the leading order of this quantity Eq. (9) is equivalent to

$$(\Omega^2-\omega_s^2)(\Omega+\Delta-j\Gamma)(\Omega-\Delta-j\Gamma)=If(\Omega), \quad (10)$$

where

$$f(\Omega)\equiv-\xi[\omega_c(\Omega-\Delta-j\Gamma)-\omega_c^*(\Omega+\Delta-j\Gamma)], \quad (11)$$

the frequency detuning $\Delta=h\omega_0-\omega_{res}$, and $\xi\equiv ek_0\alpha/T_0E_0$. Sometimes the detuning angle Θ is used in place of Δ; the two quantities are related by $\Delta\equiv\Gamma\tan\Theta$.

The characteristic equation (10) is quartic in Ω and therefore has four solutions. For small current, it gives

$$\Omega=\pm\omega_s+O(I) \quad (12)$$

for the beam mode and

$$\Omega=\pm\Delta+j\Gamma+O(I) \quad (13)$$

for the cavity mode.

The cavity mode can be understood as follows. When the bunch passes through the cavity, it excites, in addition to the equilibrium voltage with frequency $h\omega_0$, a transient voltage [9] of frequency ω_{res} with damping coefficient Γ. When these two components of the voltage act back on the bunch, the revolution harmonics of the beam are modulated by Δ. The modulated beam oscillation of frequency $h\omega_0\pm\Delta$ then feeds back on the cavity leading to the cavity Robinson mode. The cavity voltage component with frequency ω_{res} can also be excited by noise with a large bandwidth.

We end this section by discussing the symmetry properties of the solutions of the characteristic equation. Since the characteristic equation (10) represents a physical system, its solutions satisfy the reality condition. This implies that if Ω is a complex-valued coherent frequency, then so is $-\Omega^*$. The solutions appear in mirror-image pairs with respect to the imaginary axis unless they are pure imaginary. The characteristic equation must, as a consequence of this condition, have one of the following three forms:

$$P(\Omega)=(\Omega-\Omega_1)(\Omega+\Omega_1^*)(\Omega-\Omega_2)(\Omega+\Omega_2^*) \quad (14a)$$

$$=(\Omega-jy_0)(\Omega-jy_1)(\Omega-\Omega_1)(\Omega+\Omega_1^*) \quad (14b)$$

$$=(\Omega-jy_0)(\Omega-jy_1)(\Omega-jy_2)(\Omega jy_3), \quad (14c)$$

where the y's are real and Ω_1 and Ω_2 are not pure imaginary. Form (14a) represents solutions that appear in two conjugate pairs. One of the pairs, say, Ω_1 and $-\Omega_1^*$, will later be identified with the cavity mode and the other pair with the beam mode. Form (14b) represents the case where one of the two modes (e.g., the cavity mode), but not both, has two pure imaginary coherent frequencies and the other mode has conjugate-pair frequencies. Form (14c) will not be discussed.

III. STABILITY

In this section we discuss the stability of the Robinson modes described by the characteristic equation. In doing so we draw upon the work of Routh [7] that relates the sign of the imaginary part of Ω to the coefficients of the characteristic polynomial [10,11]. Routh criteria are necessary and sufficient conditions for stability and are used here to identify all the possible unstable coherent modes.

Stability criteria, conditions that require the imaginary part of solutions Ω of the equation

$$P(\Omega)=(j\Omega)^4+a_3(j\Omega)^3+a_2(j\Omega)^2+a_1(j\Omega)+a_0=0 \quad (15)$$

to be positive, are provided by Routh [7]:

$$a_3>0, \quad (16a)$$

$$(a_3a_2-a_1)/a_3>0, \quad (16b)$$

$$a_1(a_3a_2-a_1)/a_3-a_3a_0>0, \quad (16c)$$

$$a_0>0. \quad (16d)$$

Applied to the characteristic equation (10), we have the associations

$$a_3=2\Gamma, \quad (17a)$$

$$a_2=\Delta^2+\Gamma^2+\omega_s^2, \quad (17b)$$

$$a_1=2\Gamma(\xi I+\omega_s^2), \quad (17c)$$

$$a_0=2\xi I(\Gamma^2-\omega_{res}\Delta)+(\Delta^2+\Gamma^2)\omega_s^2. \quad (17d)$$

Of the four conditions (16), two are quickly understood. From Eq. (17a), the inequality (16a) is trivially satisfied. For practical reasons, Eq. (16b) is of little concern. Using the expressions for a_i in Eq. (17), we have $-\xi I+\Delta^2+\Gamma^2>0$. Using vuv numbers, this condition is satisfied unless $I>250$ A; since the ring is operated below 1 A we assume that inequality (16b) is satisfied as well. We see below that the remaining conditions (16c) and (16d) are conditions on the resistive and reactive Robinson instabilities.

A. Resistive mode

We discuss here the coherent mode that can be unstable for a very small beam current, namely, the well-known resistive mode. From Eq. (13) the cavity mode is damped at $I=0$ by the damping coefficient Γ; therefore, from continuity, the mode cannot become unstable for very small current. On the other hand, the beam mode is, from Eq. (12), neither damped nor excited at vanishing current. To the leading order of I, the damping rate Ω_I, $\Omega\equiv\Omega_R+j\Omega_I$, of this mode can be calculated from Eqs. (10) and (11) as

$$\Omega_I\propto I(-\omega_s^2\Gamma^2+\Delta^2+2\omega_{res}\Delta)+O(I^2), \quad (18)$$

with positive proportionality coefficient. The stability condition is

$$-\omega_s^2-\Gamma^2+\Delta^2+2\omega_{res}\Delta+O(I)>0. \quad (19)$$

For the vuv ring, this gives $\Delta>8$ Hz, a very small number since the bandwidth 2Γ of the cavity resonance is $\sim 4\times10^4$/s. This explains why the vuv ring is operated capacitively (just like every other electron storage ring.)

By routine substitution, the Routh inequality (16c) reduces to

$$2\xi\Gamma I(-\omega_s^2-\Gamma^2+\Delta^2+2\Delta\omega_{res}-\xi I)>0. \tag{20}$$

This inequality is seen to be the same as the stability condition (19) for the resistive mode.

B. Robinson condition

We are left with the condition (16d). This condition is fairly obvious: If

$$a_0=0, \tag{21}$$

then $\Omega=0$ is a solution of Eq. (15). Since vanishing Ω implies vanishing Ω_I, Eq. (21) is a threshold condition. Changing the current infinitesimally from the threshold current corresponding to Eq. (21), solving Eq. (15) perturbatively, and using $a_1>0$, we find that the stability condition is given by Eq. (16d).

Let us express this stability condition in terms of the detuning angle Θ. Recalling $\Gamma=\omega_{res}/2Q$ and $\Delta=\Gamma\tan\Theta$, the stability condition can be written as

$$\left(1+\frac{\Delta}{\omega_{res}}\right)\sin 2\psi_V-\rho\left(\sin 2\Theta-\frac{1}{Q}\cos^2\Theta\right)>0, \tag{22}$$

where the beam loading parameter

$$\rho\equiv P_{\text{radiation}}/P_{\text{cavity}}=I\hat{V}\cos\psi_V/(\hat{V}^2/2R_{sh}).$$

The Eq. (22) is a slightly modified Robinson condition. If the terms involving Δ/ω_{res} and $1/Q$ in Eq. (22) are ignored, we obtain the original Robinson condition

$$\sin 2\psi_V>\rho\ \sin 2\Theta.$$

Since $\pi/2>\psi_V>0$, this mode is stable if the cavity is detuned inductively, i.e., Θ and Δ are less than zero.

IV. COLLISION OF BEAM AND CAVITY MODES

The beam mode and the cavity mode for small beam current I were defined in Sec. II through Eqs. (12) and (13): The cavity mode is the mode whose frequencies $\Omega_c(\Delta,I)$ and $-$c.c. approach $\pm\Delta+j\Gamma$ continuously when the beam current approaches zero while Δ is kept fixed. From the reality condition of the eigensolutions, a solution at $\Omega=\Delta+j\Gamma$ implies its image solution at $\Omega=-\Delta+j\Gamma$. Similarly, the frequencies $\Omega_b(\Delta,I)$ and $-$c.c. of the beam mode approach $\pm\omega_s$ in the same limit. The same definition can be used for a finite beam current without ambiguity provided the coherent frequencies of the beam mode and the cavity mode do not become degenerate when the current is increased. We find below that there is one and only one such collision point of the modes (at a practical beam current) and the collision can occur only when the cavity is capacitively detuned.

We discuss form (14a) of Sec. II. Change the notation $\Omega_1\rightarrow\Omega_c$ and $\Omega_2\rightarrow\Omega_b$ to indicate, respectively, the cavity mode and the beam mode. Comparing Eqs. (14a) and (15), we have

$$\Omega_c-\Omega_c^*+\Omega_b-\Omega_b^*=ja_3.$$

Since $a_3=2\Gamma$, this relation is equivalent to the following simple but useful relationship between the imaginary parts of the mode frequencies:

$$\Omega_{cI}+\Omega_{bI}=\Gamma. \tag{23}$$

To see when the mode collision happens, let us assume that $\Omega_b=\Omega_c=\overline{\Omega}=\overline{\Omega}_R+j\overline{\Omega}_I$ when $(\Delta,I)=(\overline{\Delta},\overline{I})$; we want to solve for $\overline{\Delta}$, $\overline{I}$, and $\overline{\Omega}$. We first note that $\overline{\Omega}_I$ can be obtained simply from Eq. (23). Since $\Omega_{bI}=\Omega_{cI}=\Omega_I$ at the collision point, we have, from this equation,

$$\overline{\Omega}_I=\Gamma/2. \tag{24}$$

To go on, let us write Eq. (14a) at the collision point as

$$P(\Omega)=(\Omega-\overline{\Omega})^2(\Omega+\overline{\Omega}^*)^2. \tag{25}$$

Denoting $\overline{a}_n\equiv a_n(\overline{\Delta},\overline{I})$ for $n=0$, 1, 2, and 3, we also have the barred form of Eq. (15),

$$P(\Omega)=(j\Omega)^4+\overline{a}_3(j\Omega)^3+\overline{a}_2(j\Omega)^2+\overline{a}_1(j\Omega)+\overline{a}_0. \tag{26}$$

Comparing the coefficients of Eqs. (25) and (26), we obtain four equations for the $\overline{a}$'s in terms of $\overline{\Omega}$ and $\overline{\Omega}^*$. Elimination of $\overline{\Omega}$ and $\overline{\Omega}^*$ from these equations leads to two constraints for the two variables $\overline{\Delta}$ and $\overline{I}$:

$$(\xi\overline{I}+\omega_s^2)^2-\overline{a}_0=0 \tag{27}$$

and

$$\overline{\Delta}^2=\omega_s{}^2+2\xi\overline{I}. \tag{28}$$

For the vuv ring, these two equations give two solutions with positive current. The first one is $\overline{I}=20.27$ mA and the other is an impractical 10^{11} A. We disregard the latter solution. For the former solution, $\overline{\Delta}=70\ 208.6$ rad/s. Compare this with $\omega_s=70\ 208.0$ rad/s. The near identity of these two quantities is the result of the fact that the ratio of the term $2\xi\overline{I}$ of Eq. (28) to ω_s^2 is of the order of Γ/ω_0, which is generally very small for an electron ring. If we ignore this term, then the equation gives

$$\overline{\Delta}=\omega_s. \tag{29}$$

Continuation of this line of reasoning gives, in addition to Eqs. (29) and (24), the following results about the collision point:

$$|\overline{\Omega}|=\omega_s \tag{30}$$

and

$$\overline{I}=\Gamma^2\omega_s/2\xi\omega_{res}. \tag{31}$$

The results of this section are crucial for visualizing later the behavior of the beam and cavity modes when the cavity is detuned capacitively.

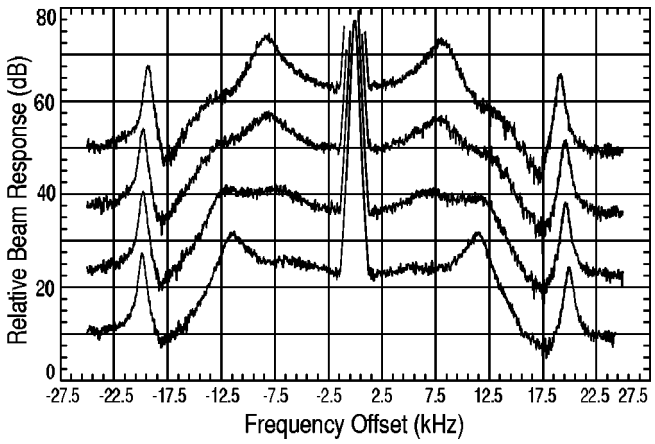

FIG. 2. Sample data set of beam responses showing the two modes of coherent motion at a 52-mA beam current. The cavity detunings for the traces are 13.1, 11.6, 10.0, and 8.8 kHz from top to bottom, respectively. One resonance is offset less than 10 kHz from the rotation line and becomes more distinct as the detuning becomes more negative. The other resonance appears above 10 kHz from the rotation line and becomes sharper as the detuning becomes more positive. The resonances have similar widths and heights in the trace second from the bottom; similar traces at different currents were assembled to form Fig. 3.

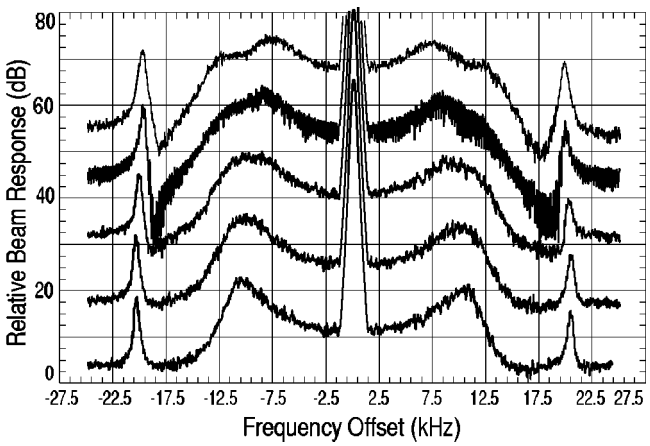

FIG. 3. Observation of the collision of the beam and cavity Robinson modes in the vuv ring. From top to bottom, the five traces have beam current and detuning $(I,\Delta/2\pi)=(58$ mA, 10.3 kHz), (42 mA, 11.8 kHz), (31 mA, 11.3 kHz), (26 mA, 11.0 kHz), and (21 mA, 10.8 kHz). Although the resonances are not clearly separated as they are in Fig. 2, each of the traces was taken from a data set similar to that figure where the modes were easily distinguished at other detunings. In this figure the final stage of the collision is shown where the two modes merge together at a collision point between 26 and 21 mA.

We were able to observe the mode collision in the vuv ring and verify that its location is close to the values determined from Eqs. (29) and (31). The responses of the beam as a function of frequency to longitudinal excitation by a broadband cavity were taken at different detuning and currents approaching the collision point. Figure 2 shows a sample data set taken at a current well above the collision point where the real parts of the beam- and cavity-mode frequencies are well separated; the beam- and cavity-mode resonances are on both sidebands on either side of the 10-kHz offset from the rotation line. (There is also a quadrupole resonance at about 20-kHz offset.) The collision must occur when the widths (and heights) of the resonances are similar. In Fig. 3 traces taken from different data sets having different detuning and currents approaching $(\overline{\Delta},\overline{I})$ are assembled. In the traces where the beam- and cavity-mode resonances are not clearly separated, they were confirmed to be present by inspection of the original data sets, e.g., Fig. 2. Figure 3 shows the merging of the two resonances near 10-kHz offset, a value near ω_s inferred from the location of the quadrupole resonances and from the reduced cavity voltage (73 kV). Although data were not taken at beam currents below 21 mA, the collision appears to be between 26 and 21 mA.

V. GRAPHIC REPRESENTATION

We discuss in this section the parametric (Ω_R,Ω_I) plot of the solutions of Eq. (15). For each plot, Δ (or equivalently Θ) is fixed and the beam current I is the parameter. These plots will be referred to as the solution curves or the solution loci. The examples considered are based on the vuv ring parameters given in Table I.

A. Inductive case $\Theta<0$

It suffices to plot three examples corresponding to $\Delta=2\pi\times-3.4$, -12.8, and -28.0 kHz ($\Theta=-47°$, $-76°$, and $-83°$, respectively) in Fig. 4 since these curves are representative of the inductive case. The fine-dashed (leftmost) pair of curves corresponds to $\Delta=2\pi\times-3.4$ kHz, the coarse-dashed (center) curves correspond to $\Delta=2\pi\times-12.8$ kHz, and the uneven-dashed (right-most) curves correspond to $\Delta=2\pi\times-28.0$ kHz. The solid horizontal line in the figure corresponds to $\Omega_I=\Gamma$. The cavity-mode frequencies (the broken lines on the upper half plane) fall on this line at $I=0$ and move upward (become more damped) with increasing current. The beam-mode frequencies (the broken curves on the lower half plane) start at ω_s and move downward (become increasingly unstable) with increasing current.

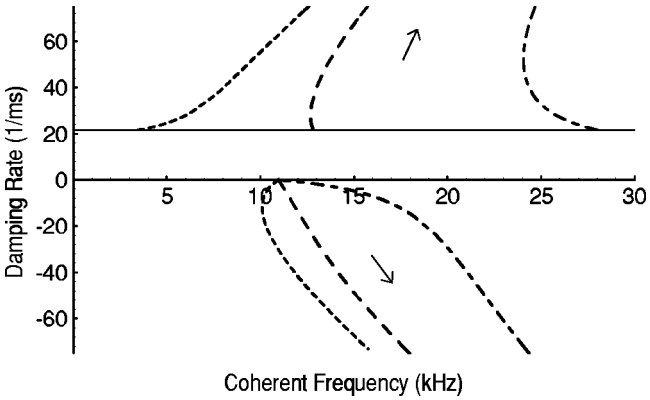

FIG. 4. Parametric plots on the complex-Ω plane of solutions of Eqs. (10) and (11) for the NSLS vuv ring with an inductively detuned cavity. The beam current is varied along each curve; the arrows give the direction of increasing current. The solid horizontal line corresponds to $\Omega_I=\Gamma$, the damping rate of the cavity rf mode. The broken curves with negative damping rates are the beam-mode frequencies Ω_b and the others are the cavity-mode frequencies Ω_c. The three beam-mode, cavity-mode pairs are, from left to right, for $\Delta=2\pi\times-3.4,-12.8$, and -28.0 kHz.

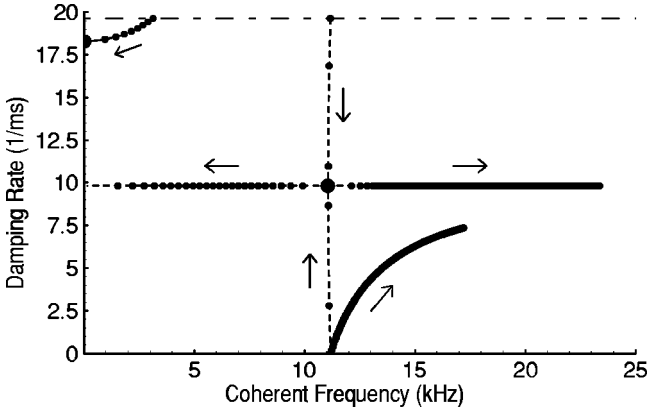

FIG. 5. Confluence curves on the complex-Ω plane for the NSLS vuv ring where the cavity detuning $\Delta=\bar{\Delta}=2\pi\times 11.2$ kHz (dashed curves) and beam- and cavity-mode coherent frequencies for $\Delta=2\pi\times 3.2$ kHz (solid curves). The beam- and cavity-mode collision point is the large central dot at $I=\bar{I}=20.3$ mA. The cavity-mode frequency approaches the collision from above, starting at $\Omega=\omega_s+j\Gamma$, while the beam-mode frequency approaches from below, starting at $\Omega=\omega_s$. The small dots mark beam-current increments of 10 mA. The cavity damping rate Γ is marked with the upper broken line at a damping rate 19.6/ms.

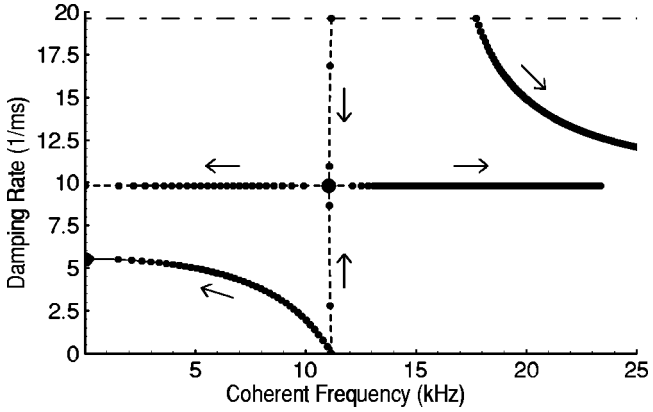

FIG. 6. Confluence curves on the complex-Ω plane for the NSLS vuv ring where the cavity detuning $\Delta=\bar{\Delta}=2\pi\times 11.2$ kHz (dashed curves) and beam- and cavity-mode coherent frequencies for $\Delta=2\pi\times 17.7$ kHz (solid curves). The small dots mark beam-current increments of 10 mA. The cavity damping rate Γ is marked with the upper broken line at a damping rate 19.6/ms.

The condition (23) requires that the two modes cannot both become more unstable with increasing current. It is also important to note that the cavity- and beam-mode frequencies are separated from each other by a gap located at $0<\Omega_I<\Gamma$. This explains why a collision point with negative Δ was not found in Sec. IV.

B. Capacitive case $\Theta>0$: Confluence curves

It was seen in the Sec. IV that there is a unique pair of mode collision points Ω and $-\Omega^*$ that are not pure imaginary. Such a mode collision occurs only for capacitive detuning $\Delta=\omega_s>0$ and the current is given by Eq. (31). The solution curves that pass through the collision point Ω are referred to as confluence loci or confluence curves. In terms of the detuning angle, $\Delta\equiv\Gamma\tan\Theta$.

For the vuv ring, $\Theta=74.4°$, $\Delta=\omega_s=2\pi\times 11.2$ kHz, and $\bar{I}=20.3$ mA. In Figs. 5 and 6 the dashed curves are the confluence curves and the central dots represent the collision point (Ω_R,Ω_I). The dash-dotted lines again correspond to $\Omega_I=\Gamma$.

These pictures require some additional explanation. The confluence curves divide the region $\Omega_R>0$, $\Omega_I>0$ in the complex plane into four regions. For $\Delta>\bar{\Delta}$ (solid curve of Fig. 6), the beam mode occupies the lower-left quadrant and the cavity mode occupies the upper-right quadrant. When the beam current I increases, the damping rate Ω_I of the beam mode increases while that of the cavity mode decreases such that the condition (23) is maintained. The real part of the cavity-mode frequency increases with increasing current and that of the beam mode moves towards and eventually collides with its own image on the imaginary Ω axis. For $\Delta<\bar{\Delta}$ (solid curve of Fig. 5), the situation is just the opposite: The beam mode occupies the lower-right quadrant and the cavity mode occupies the upper-left quadrant. The locus of the cavity mode moves towards the imaginary axis with increasing current and eventually reaches the imaginary axis colliding with its own image. The pure imaginary collision points are also represented by dots in the figures.

We now consider the case corresponding to Fig. 5 where the beam current is further increased after the mode collision on the imaginary axis; the case of Fig. 6 is similar. After the collision, the two coherent frequencies corresponding to the cavity mode both become pure imaginary, no longer mirror images of each other; the characteristic polynomial will take the form (14b). The two pure imaginary coherent modes after collision are depicted in Fig. 7; the black dot corresponds to the collision point on the imaginary axis. We see from this figure that one of the coherent frequencies vanishes when $I\sim 145$ mA. This is the threshold current corresponding to the Robinson condition (21). When $\Delta>\bar{\Delta}$, it is the beam mode whose coherent frequency becomes pure imaginary for large current and the threshold current for the reactive instability is again given by Eq. (21).

Figure 8 plots the Robinson condition (21), Δ against I. The dash-dotted line corresponds to $\Delta=\bar{\Delta}=\omega_s$. The part of

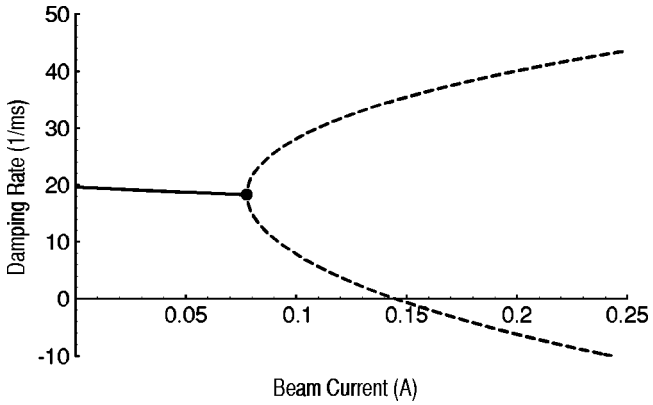

FIG. 7. Cavity-mode damping rate as a function of current showing a collision that occurs on the imaginary axis (large dot), after which the conjugate mode frequencies split to form two unequal imaginary frequencies (dashed line). The detuning $\Delta=2\pi\times 3.1$ kHz.

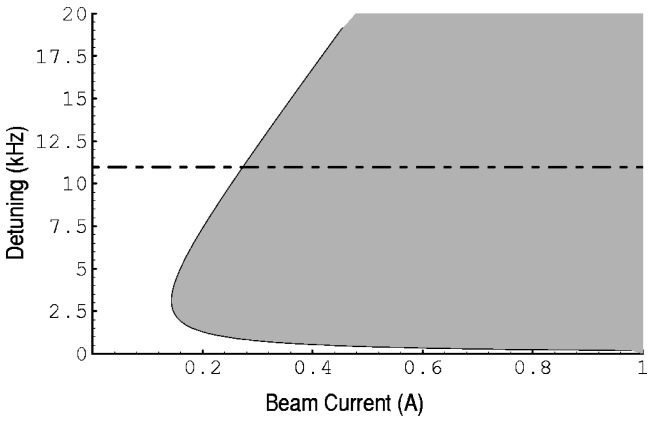

FIG. 8. Threshold condition $a_0=0$ for the reactive Robinson instability constraining current I and detuning Δ. The dash-dotted line corresponds to $\Delta=\overline{\Delta}$. The shaded region is unstable.

the curve under the dash-dotted line corresponds to $\Delta<\overline{\Delta}$ and therefore gives the threshold condition for the cavity mode. The threshold condition for the beam mode is given by the curve above the dash-dotted line. We see from this figure that the lowest threshold current ~ 145 mA for the cavity mode occurs at $\Delta\sim 2\pi\times 3$ kHz and the lowest threshold current for the beam mode ~ 280 mA occurs at $\Delta=\overline{\Delta}=2\pi\times 11.2$ kHz.

VI. CONCLUSION

In this paper we have described the properties of the longitudinal dipole modes when the impedance responsible is that of a cavity resonance mode and made a distinction between the beam Robinson mode and the cavity Robinson mode. The behavior of each of these modes was described in terms of the solution locus corresponding to a given Δ and varying I. In principle, there is a cavity mode associated with each cavity rf mode in the ring, although only rf modes with damping rate and detuning of order ω_s couple to the beam sufficiently strongly to produce observable Robinson modes.

For inductive detuning, we showed that the beam mode and the cavity mode do not mix since the beam mode occupies the region $\Omega_I<0$ in the complex Ω plane while the cavity mode occupies the region $\Omega_I>\Gamma>0$. For capacitive detuning, we showed where a collision between the beam and the cavity mode (total degeneracy) occurs and showed how the confluence of the beam- and the cavity-mode-solution loci around the total degeneracy point divides the Ω plane into beam- and cavity-mode regions. Data from the vuv ring were presented that show the mode collision verifying that it occurs at approximately the theoretical current and detuning.

Although the stability thresholds of both the beam and the cavity modes, in different kinematic regions, are given by the same condition (21) and instability is not an immediate problem, it is important in the vuv ring to choose an appropriate range of detuning so that the coherent mode does not cause excessive perturbation on the photon beam. It should be noted that the coherent modes can carry on forced oscillations driven by the ever present noise even below the instability current threshold and thus affect the photon beam quality, particularly in a ring with noisy rf systems.

In a ring with a high-Q rf system, the coupling between the beam synchrotron motion and the cavity resonance mode is intimate, even at low current. As such, even though a perturbative method can be useful for estimating the threshold of a coherent instability, it is not very useful in the calculation of the actual coherent frequency. Direct solution of equations like Eq. (6) or (10) is necessary for determining the mode frequency reliably.

ACKNOWLEDGMENT

This work was performed under the auspices of the U.S. Department of Energy under Contract No. DE-AC02-76CH00016.

[1] R. Biscardi, G. Ramirez, G. P. Williams, and C. Zimba, Rev. Sci. Instrum. **66**, 1856 (1995).
[2] K. W. Robinson, Cambridge Electron Accelerator Laboratory Report No. CEAL-1010, 1964 (unpublished).
[3] M. Sands, Laboratoire de l'Accélérateur Linéaire Report No. LAL-RT-2-76, 1976 (unpublished).
[4] B. C. Craft III, in *1985 Particle Accelerator Conference, Accelerator Engineering and Technology*, edited by A. Strathdee, IEEE Transactions on Nuclear Science Vol. NS-32, No. 5 (IEEE Nuclear and Plasma Sciences Society, Vancouver, BC, Canada, 1985), p. 2525.
[5] A. W. Chao, *Physics of Collective Beam Instabilities in Accelerators* (Wiley, New York, 1993).
[6] J.-M. Wang, in *Physics of Particle Accelerators*, edited by M. Month and M. Dienes, AIP Conf. Proc. No. 153 (AIP, Stanford, CA, 1984), Vol. 1, p. 697.
[7] See, e.g., M. E. Van Valkenburg, *Network Analysis* (Prentice-Hall, Englewood Cliffs, NJ, 1955), Chap. 16.
[8] N. Towne and J. M. Wang (unpublished).
[9] S. Kramer and J. M. Wang (unpublished).
[10] S. Koscielniak, in *Proceedings of the 1993 Particle Accelerator Conference*, edited by S. T. Corneliussen (IEEE and APS, Washington, D.C., 1993), Vol. 5, p. 3506.
[11] T.-S. F. Wang, in *Proceedings of the 1993 Particle Accelerator Conference*, edited by S. T. Corneliussen (IEEE and APS, Washington, D.C., 1993), Vol. 5, p. 3500.